A Ground Validation Network for the Global Precipitation Measurement Mission

MATHEW R. SCHWALLER

Global Precipitation Measurement Project, NASA Goddard Space Flight Center, Greenbelt, Maryland

K. ROBERT MORRIS

Global Precipitation Measurement Project, NASA Goddard Space Flight Center, Greenbelt, and Science Applications International Corporation, Beltsville, Maryland

(Manuscript received 9 October 2009, in final form 20 October 2010)

ABSTRACT

A prototype Validation Network (VN) is currently operating as part of the Ground Validation System for NASA's Global Precipitation Measurement (GPM) mission. The VN supports precipitation retrieval algorithm development in the GPM prelaunch era. Postlaunch, the VN will be used to validate GPM spacecraft instrument measurements and retrieved precipitation data products.

The period of record for the VN prototype starts on 8 August 2006 and runs to the present day. The VN database includes spacecraft data from the Tropical Rainfall Measuring Mission (TRMM) precipitation radar (PR) and coincident ground radar (GR) data from operational meteorological networks in the United States, Australia, Korea, and the Kwajalein Atoll in the Marshall Islands. Satellite and ground radar data products are collected whenever the PR satellite track crosses within 200 km of a VN ground radar, and these data are stored permanently in the VN database. VN products are generated from coincident PR and GR observations when a significant rain event occurs.

The VN algorithm matches PR and GR radar data (including retrieved precipitation data in the case of the PR) by calculating averages of PR reflectivity (both raw and attenuation corrected) and rain rate, and GR reflectivity at the geometric intersection of the PR rays with the individual GR elevation sweeps. The algorithm thus averages the minimum PR and GR sample volumes needed to ''matchup'' the spatially coincident PR and GR data types. The result of this technique is a set of vertical profiles for a given rainfall event, with coincident PR and GR samples matched at specified heights throughout the profile.

VN data can be used to validate satellite measurements and to track ground radar calibration over time. A comparison of matched TRMM PR and GR radar reflectivity factor data found a remarkably small difference between the PR and GR radar reflectivity factor averaged over this period of record in stratiform and convective rain cases when samples were taken from high in the atmosphere. A significant difference in PR and GR reflectivity was found in convective cases, particularly in convective samples from the lower part of the atmosphere. In this case, the mean difference between PR and corrected GR reflectivity was -1.88 dBZ. The PR–GR bias was found to increase with the amount of PR attenuation correction applied, with the PR–GR bias reaching -3.07 dBZ in cases where the attenuation correction applied is >6 dBZ. Additional analysis indicated that the version 6 TRMM PR retrieval algorithm underestimates rainfall in case of convective rain in the lower part of the atmosphere by 30%–40%.

1. Introduction

In collaboration with its international partners, National Aeronautics and Space Administration (NASA) is developing a Ground Validation System (GVS) as a contribution to the Global Precipitation Measurement (GPM) mission. In the United States, GPM has been recognized as a key weather and climate mission for providing uniform, global precipitation products that leverage all available satellites capable of precipitation measurement (NAS 2007). In achieving these goals, GPM addresses the call for ''essential climate variables,'' as defined by the Global Climate Observing System (GCOS 2006). The GPM framework is also intended to be a realization of a ''precipitation constellation'' of satellites and ground-based assets that will deliver fundamental climate data records for social benefit (Neeck and Oki 2007).

Corresponding author's address: Mathew R. Schwaller, Mail Code 422/587, Global Precipitation Measurement Project, NASA Goddard Space Flight Center, Greenbelt, MD 20771.
E-mail: mathew.r.schwaller@nasa.gov

DOI: 10.1175/2010JTECHA1403.1

The international GPM mission extends observations of the Tropical Rainfall Measuring Mission (TRMM; Simpson et al. 1996; Kummerow et al. 2000) to precipitation at higher latitudes, with more frequent sampling, and with research focused on a more complete understanding of the global hydrological cycle. It is expected that the dual-frequency precipitation radar (DPR) instrument on board GPM will be capable of measuring rain rates from ~0.2 to 110 mm h^{-1}. GPM DPR products will estimate the sizes of precipitation particles and the drop size distribution (DSD) of rain, using the attenuation difference between the Ka- and Ku-band frequencies in the DPR, and they will also discriminate between snow and rain. Mission requirements specify that GPM precipitation products will be available with a 3-h average revisit time over 80% of the globe, and data will be available to users within 3 h of observation (Hou et al. 2008).

In support of the international GPM, NASA is planning to launch a GPM core satellite into a medium (65°) inclination orbit no later than July 2013. Current plans call for the GPM GVS to support the GPM satellite mission. In the prelaunch era, the GPM GVS provides data to support the development of precipitation retrieval algorithms. In the postlaunch era, the GPM GVS provides an independent means for evaluation, diagnosis, and ultimately improvement of GPM space-borne measurements and precipitation products.

This paper specifically describes one component of the GPM GVS: a Validation Network (VN) that compares GPM DPR data products to similar measurements and products from national networks of operational weather radars. The main focus of the VN work described below is the direct comparison of radar reflectivity factor data generated by ground- and space-based radars. Reflectivity factor was selected because it is the fundamental product used in radar precipitation retrievals. The ultimate goal of the VN is to understand and resolve the first-order variability and bias of precipitation retrievals in different meteorological and hydrological regimes at large scales. Although the VN is intended for GPM validation, an initial version of the system is now in operation that uses TRMM satellite data. The current version of the VN is built on methods, research results, and computer code described by Anagnostou et al. (2001), Bolen and Chandrasekar (2000), Liao et al. (2001), and Bolen and Chandrasekar (2003).

As part of the international GPM mission, the VN is designed to incorporate and exploit data contributed by an arbitrary number of national meteorological networks of ground radars. At present, the VN includes contributions from ground radars located in Australia, South Korea, the Kwajalein Atoll in the Marshall Islands, and the southeastern United States. However, the system, as described below, was designed to be readily scalable. Thus, the VN allows for the inclusion of new radars and additional national networks with only minor modification to the VN code and database tables. Future plans call for the inclusion of spacecraft microwave radiometer data into the VN.

2. VN data sources

The current period of record for the VN data starts on 8 August 2006 and runs to the present day. The current VN database includes spacecraft data from the TRMM precipitation radar (PR) and coincident ground radar (GR) data from several sources, as described below. Satellite and ground radar data products are collected whenever the PR satellite track crosses within 200 km of a VN ground radar, and these data are stored permanently in the VN database. The generation of VN products from the coincident PR and GR datasets, however, occurs only when there is a "significant rain event," as defined in section 3. Because many of the ground radar datasets are quality controlled by a human analyst prior to ingest into the VN, there is a variable time lag between observation and VN product creation.

a. TRMM PR

PR data are extracted from standard TRMM version 6 data products—1C-21, 2A-23, 2A-25, and 2B-31—for orbital overpass events where the instrument ground track coincides with a VN ground radar. The extracted PR data include radar reflectivity (both raw and attenuation corrected), near-surface rain rate, and other variables (see section 4). The VN acquires these data as orbit subset products directly from NASA's Precipitation Processing System (PPS; online at http://pps.gsfc.nasa.gov/pps). The PR data, along with detailed product descriptions, are also available to the public via NASA's Goddard Earth Sciences (GES) Data and Information Services Center (DISC; online at http://disc.sci.gsfc.nasa.gov).

At the current TRMM orbital altitude of 402 km, the 13.8-GHz (Ku band) PR data are characterized by a ground-level instantaneous field of view of approximately 5 km. The instrument scans along the satellite cross-track direction to yield a 247-km swath, with 49 ray samples in each cross-track scan. Within each ray, the PR samples a column of the atmosphere in series of range bins, each with a vertical resolution of 250 m, from ground level up to 20 km (Kozu et al. 2001).

b. WSR-88D

At present, the VN acquires ground radar data for 21 of the 59 National Oceanic and Atmospheric Administration (NOAA)- and Department of Defense (DoD)-operated Weather Service Radar-1988 Doppler [WSR-88D; Next Generation Weather Radar (NEXRAD)]

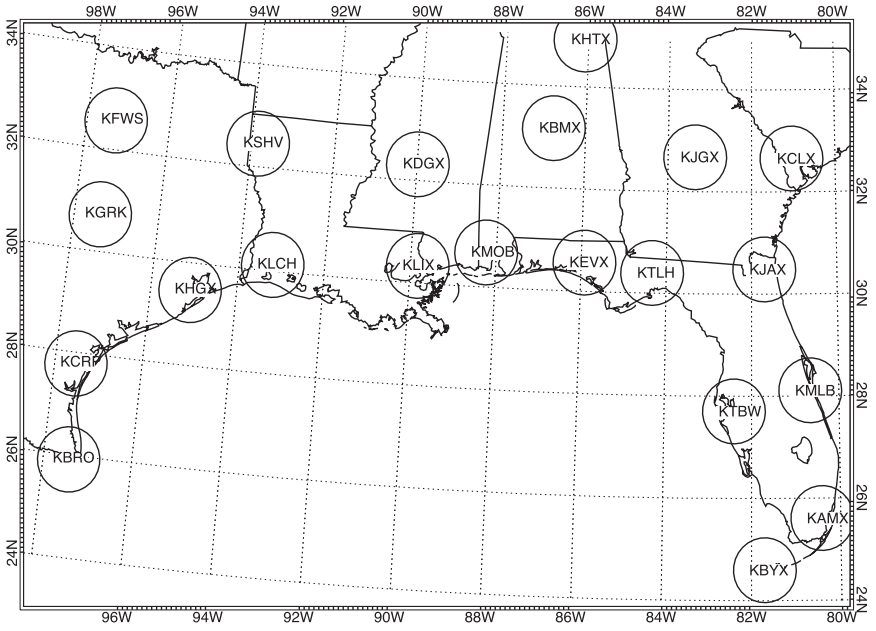

FIG. 1. Location of VN WSR-88D matchup sites in the southeastern United States; 100-km observation limits are illustrated for each site.

radar sites in the continental United States that are within view of the PR instrument. This 21-site subset falls within a bounding area with latitudes below 33°N and longitudes east of 98°W, plus KHTX (see Table 1) at 34.9°N, 86.1°W (see Fig. 1 and Table 1). Raw data are acquired from the WSR-88D level II archive. In addition, the VN acquires WSR-88D data for these sites that have been quality controlled via the methods applied to the TRMM standard ground validation product 1C-51. The 1C-51 algorithm includes screening by automated methods and by an analyst to remove nonmeteorological radar echoes, such as clutter associated with insects, birds, chaff, wildfires, antenna towers, and anomalous propagation (Rosenfeld et al. 1995; Wolff et al. 2005). Data ingested from these sources include the radar reflectivity factor, near-surface rainfall, and derived variables.

The WSR-88D radars operate at S band (2.7–3.0 GHz), and scan using a variety of weather-dependent standard volume coverage patterns. Data are collected as 360° full scans at a varying number of elevation angles from 0.5° to 19.5°, with gaps between the half-power beamwidth dimensions growing with elevation angle. The WSR-88D products used in the VN provide sample volumes with a range resolution of 1 km and an azimuth resolution of 1°. The typical WSR-88D precipitation mode volume scan repeats every 4–6 min (NOAA/OFCM 2006).

c. Gosan radar

Data from the Gosan radar, located on the western tip of Jeju Island, were provided to the VN by the National Institute of Meteorological Research (METRI) of the Korea Meteorological Administration (KMA). KMA operates a total of 12 C- and S-band radars within South Korea. These, together with radars operated by the Korean Air Force and the U.S. Air Force, constitute an operational network of 18 radars covering the whole of the southern Korean Peninsula. At present, data from the radar at Gosan have been ingested into the VN. The Gosan radar (RSGN) is an S-band radar operating with a range resolution of 0.125 km and an azimuth resolution of about 1°, and a nominal range of 250 km. The Gosan radar carries out one volume scan at 10–15 elevation angles from 0° to 45° every 10 min (Park and Lee 2007).

d. ARMOR radar

The Advanced Radar for Meteorological and Operational Research (ARMOR) is a scanning dual-polarimetric Doppler radar operating in simultaneous transmit–receive mode at C band (5625 MHz) with a beamwidth of 1°. ARMOR was originally deployed in Huntsville, Alabama, by the National Weather Service in 1977 as a Weather Surveillance Radar-1974 C band (WSR-74C) local warning radar, which was refurbished and upgraded to Doppler in 1991. The radar was donated to the Department of Atmospheric Science at the University of Alabama, Huntsville in 2002, and upgraded to dual polarimetry using the Significant Meteorological Information (SIGMET) Antenna Mounted Receiver in the fall of 2004; a new antenna system was added in 2006 (Petersen et al. 2007).

TABLE 1. Ground radar sites included in the current GPM GVS VN. Sites listed in *italics* are not part of the NOAA WSR-88D network.

Site ID	Site name	Lat (°N)	Lon (°E)
KAMX	Miami, FL	25.6111	−80.4128
KBMX	Birmingham, AL	33.1722	−86.7697
KBRO	Brownsville, TX	25.9161	−97.4189
KBYX	Key West, FL	24.5975	−81.7031
KCLX	Charleston, SC	32.6556	−81.0422
KCRP	Corpus Christi, TX	27.7842	−97.5111
KDGX	Jackson, MS	32.3178	−89.9842
KEVX	Eglin Air Force Base, FL	30.5644	−85.9214
KFWS	Dallas–Fort Worth, TX	32.5731	−97.3031
KGRK	Fort Hood, TX	30.7219	−97.3831
KHGX	Houston, TX	29.4719	−95.0792
KHTX	Huntsville, AL	34.9306	−86.0833
KJAX	Jacksonville, FL	30.4847	−81.7019
KJGX	Robins AFB, GA	32.6753	−83.3511
KLCH	Lake Charles, LA	30.1253	−93.2158
KLIX	Slidell, LA	30.3367	−89.8256
KMLB	Melbourne, FL	28.1133	−80.6542
KMOB	Mobile, AL	30.6794	−88.2397
KSHV	Shreveport, LA	32.4508	−93.8414
KTBW	Tampa Bay, FL	27.7056	−82.4017
KTLH	Tallahassee, FL	30.3975	−84.3289
RGSN	*Gosan, Korea*	*33.2942*	*126.1630*
RMOR	*ARMOR, Huntsville, AL*	*34.6460*	*−86.7700*
DARW	*Darwin, QSL, Australia*	*−12.2522*	*131.0430*
KWAJ	*Kwajalein Atoll*	*8.7180*	*167.7330*

e. Darwin radar

The Australian Bureau of Meteorology (BOM) operates the Darwin (DARW) C-band (5625 MHz) dual-polarization Doppler radar (C-POL; Keenan et al. 1998), with a beamwidth of 1° and polarimetric capability.

f. Kwajalein radar

The Kwajalein radar (KWAJ) is a modified Weather Surveillance Radar-1993 (WSR-93) S-band (2780 MHz) scanning radar with a beamwidth of 1.12° and Doppler and dual-polarization capability upgrades. It is described in detail in Schumacher and Houze (2000) and Wolff et al. (2005).

3. VN software description

The VN software suite consists of the following three major components: 1) data ingest and preprocessing, 2) the resampling of PR and GR to common three-dimensional data volumes (the creation of matchup data products), and 3) the statistical analysis and display of the matching data volumes.

The data ingest and preprocessing component of the VN software ingests and stores TRMM PR and coincident ground radar data whenever an "overpass event" occurs. Such an event takes place any time the TRMM PR ground track passes within 200 km of a VN GR site. For each overpass event, the earliest GR volume scan, beginning within a 9-min window centered on the satellite overpass time, is acquired, along with its corresponding PR data. GR data are acquired for the WSR-88D sites on a routine, operational basis by the VN, via NASA's TRMM Ground Validation Office. Data for other the ground radar sites are currently acquired by the VN on an ad hoc basis from the data providers. Subsets of the full-orbit PR data provided by the PPS for single radars or adjacent groups of radars are acquired by the VN. All data acquired by the VN are stored permanently in the VN file system, unmodified and in their native format. All of the acquired data files are cataloged in the VN in a PostgreSQL relational database.

Selected fields of the PR products are analyzed upon receipt to temporary 75 × 75 point Cartesian grids of 4-km resolution aligned to local north, with one centered on each ground radar site overpassed by the TRMM satellite in the given orbit. The VN software harvests metadata parameters for each site-overpass event from the temporary grids. These parameters serve to characterize the precipitation and radar echo characteristics of the event, and the gridding method allows for backward compatibility with legacy grid-based methods of PR and GR volume matching. Metadata are stored in the VN relational database and are linked through the database to the associated PR orbit subset and GR data files. The stored metadata parameters include the average height of the bright band over the analysis area and the number of grid points, as follows:

- total, in a horizontal grid slice;
- covered by the PR data swath: total for grid, and total within a 100-km radius of the GR site;
- indicating rain certain: total, and within 100 km;
- indicating convective rain type: total, and within 100 km;
- indicating stratiform rain type: total, and within 100 km
- indicating rain type "other": total, and within 100 km;
- indicating no rain: total, and within 100 km; and
- indicating bright band exists: total, and within 100 km.

The time and distance of the nearest approach of the TRMM orbit track to the ground radar site and the start time of the GR volume scan are also stored in the database. Queries to the database allow an analyst to easily identify events with significant areal precipitation, events of a given predominant rain type (convective, stratiform, or unknown), or precipitation events where the orbital track is within a threshold distance of the ground radar. All associated PR and GR data files are cataloged in the database and linked to the site-overpass events, making it easy to identify and assemble associated data files for significant events. Most site-overpass events will have no occurrence of precipitation echoes. The preprocessed

metadata in the database makes it easy to select rainy overpass events without the need to process all of the data or make complicated time–space associations to external data sources.

On average, about 48 coincident events with available matching PR and GR data are collected each month for each of the WSR-88D ground radars listed in Table 1. Because of their proximity to the top of the TRMM orbit, the northernmost sites in the table experience about twice the number of coincident overpasses as the southernmost sites.

Although PR and GR data products from every overpass event are acquired and stored, PR-to-GR matchup products are generated only when an overpass event occurs during a ''significant precipitation event,'' as indicated in the stored metadata for the event. A significant precipitation event is defined as one in which at least 100 grid points (in total; not necessarily contiguous) within 100 km of the radar indicate ''rain certain'' (as defined in the PR product 2A-25). In the period from 8 August 2006 through 25 March 2009, a total of 32 244 coincident overpass events at the WSR-88D sites were recorded by the VN. Of these, 2478 events met the significant precipitation criteria, and 2292 of these had matching GR data available. Thus, per site and per month, about four coincidence events meet the criteria for a VN rainfall event, and about 3.5 per month of these have both PR and GR data.

The resampling component of the VN software suite performs a geometric matchup of the PR and GR data for the significant precipitation events. In this method, described in detail in section 4, common 3D volumes are defined by the intersection of the individual PR rays with the each of the conical elevation sweeps of the ground radar for the time—space-coincident GR volume scan. Thus, the resampled volume elements of the VN PR and ground radars can be directly compared. An earlier ''legacy'' version of the VN software involves resampling the data to a fixed 3D Cartesian grid centered on the radar site, following the analysis procedures described in Liao et al. (2001). Both the legacy and the current matchup software store the resulting PR-to-GR ''matchups'' as Network Common Data Form (netCDF) files in the VN file system. The remainder of this paper is restricted to descriptions and results pertaining to the current geometric matchup version of the VN algorithm.

A statistical analysis and display component of the VN software suite generates statistical comparisons and graphical displays of PR and GR reflectivity factor and rain rate from the volume-matched data for a wide variety of data classifications. In many of the analysis and display programs, the data and results may be classified by individual attributes or combinations of attributes stored as, or derived from, variables stored within the netCDF files or the VN database. Attributes may apply to the entire data file, to a subset of the data in the file, or to an individual matchup sample volume. The primary attributes on which the data are classified typically include the following:

- GR site,
- date–time ranges,
- height above the surface,
- proximity to the bright band (above, below, within),
- precipitation type (stratiform, convective, other),
- underlying surface (land, water, coast/mixed),
- range from the ground radar,
- percent completeness of the data volumes (expected versus rejected gates, based on detection thresholds), and
- time difference between the PR and GR observations.

4. VN netCDF product generation

The current algorithm to match PR and GR reflectivity data is based on calculating PR and GR averages at the geometric intersection of the PR rays with the individual GR radar elevation sweeps. By convention, the intersection points processed in the matchup are restricted to those where the intersection of the PR ray with the earth surface is within a 100-km radius of the GR site (Fig. 1). By 115-km range, radar systems such as WSR-88D (1° beamwidth) will have a vertical resolution >2 km, which is considered too coarse for meaningful comparisons with the PR data.

The matchup method averages PR and GR full-resolution space and ground radar bins within the minimum volume needed to produce a spatially coincident sample. The along-ray PR data are averaged only in the vertical, between the top and bottom height of each GR elevation sweep it intersects (Fig. 2). PR data from the clutter region near the surface are not excluded from the reflectivity averages, except where PR range gates in the 2A-25 attenuation-corrected reflectivity have been set to ''missing.'' The GR data are averaged only in the horizontal within the individual elevation sweep surfaces, over an approximately circular area centered on each intersecting PR ray's parallax-adjusted profile (Fig. 3). Reflectivity is converted (from dBZ to Z) before averaging, and then the average Z is converted back to dBZ. The output of this technique is a set of quasi-vertical profiles for a given rainfall event aligned along PR rays, with coincident PR and GR samples located at essentially random heights along each individual profile where the PR ray intersects the GR sweeps. The vertical and horizontal locations of the samples are not fixed because of the orbit-by-orbit variability of the PR viewing angles and locations with respect to the ground radar scans;

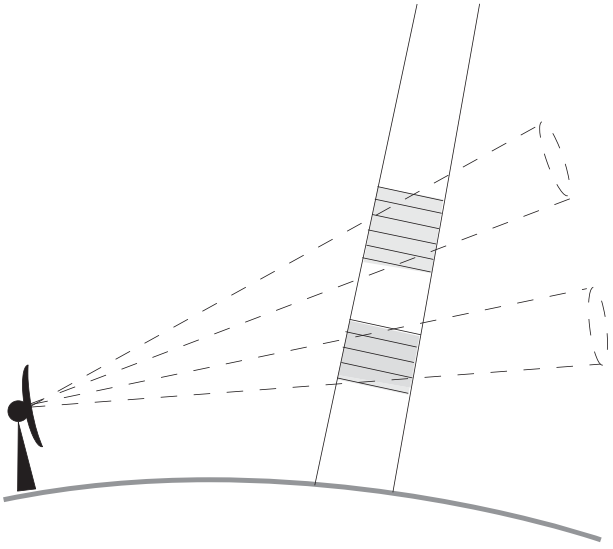

FIG. 2. Schematic of PR gate averaging at GR sweep intersections. Shaded areas are PR gates intersecting two GR sweeps (dashed) at different elevation angles. Only one PR ray is shown.

there is no resampling to a regular grid. The advantages of the current technique over gridded approaches are that there is no interpolation, extrapolation, or oversampling of the data, so matching volumes only exist at locations where both the PR and GR instruments have taken actual observations. Other than for the averaging required to produce the matching volumes, the data are not smoothed. Each sample volume carries a set of attributes that describe the precise spatial, temporal, and quality characteristics of the sample.

The VN software assigns the start time of each elevation sweep of the GR volume scan as the observation time for each sample of ground radar data within the sweep. For PR data, the time associated with each sample is the time of the PR's nearest approach to the ground radar as provided in a site coincidence table produced by the PPS. The orbital period of the TRMM spacecraft is 92.5 min, which yields a ground speed of about 7.22 km s^{-1}. At that rate, the spacecraft ground track traverses a nominal ground radar area of 200 km extent in only 28 s. This period is akin to a ''snapshot'' in comparison to either the time period required for the ground radar to complete its full volume scan, or the random time offset between the GR volume scan start time and the PR overpass. The time difference between PR and GR samples is one of the potential sources of error in the matchup of meteorological events observed by these two datasets.

In summary, the PR data resolution is reduced in the vertical to the resolution of the GR, which varies with range from the ground radar, and varies in vertical coverage by the number of elevation sweeps of the ground radar. The GR data resolution is simply reduced and remapped in the horizontal to the PR's horizontal resolution and (ray and scan) coordinate system.

The input GR product consists of quality-controlled reflectivity data in either Universal Format (UF) data files (Barnes 1980), a TRMM GV 1C-51 Hierarchical Data Format (HDF) file, or a legacy-format WSR-88D level II archive data file (i.e., pre-super-resolution), each of which contains data for a single, complete volume scan.

VN output products are in the form of binary netCDF files containing the volume-matched PR and GR data. Each VN netCDF data file corresponds to a single site-overpass event and contains all of the matchup data for the significant rain event. The basic structure of the VN netCDF matchup files is the same for all events. However, the dimensions of the data contained in the files vary, depending on the number of PR footprints that fall within a 100-km radius of the overpassed GR site for a given overpass event, and the number of unique elevation sweeps contained in the GR volume scan. In addition, the vertical and horizontal locations of the data points are unique for each event, and for each point within the event.

Horizontal and vertical positions of each data point in the geometry-matching dataset vary for each site-overpass event as a function of the TRMM orbital track and the ground radar's scan strategy (volume coverage pattern). Thus, each geometrically coincident PR and GR reflectivity data point in a given event has a unique set of associated horizontal and vertical position-variable values. All of the latitude and longitude values are parallax corrected for PR viewing angle and sample height. Multilevel variables in the dataset (e.g., rain rate; number of 2A-25 gates expected or rejected, see below) also have associated variables specifying the x and y corners of the PR footprint (km; defined relative to a Cartesian coordinate system centered at the location of the ground radar, with the $+y$ axis pointing due north), and the top and bottom height of the ground radar elevation sweep at the PR ray intersection point, in kilometers above the surface. The PR footprint ''corners'' are defined as the midpoint between the footprint center point and the centers of the four diagonally adjacent PR footprints, and are used only for graphical plotting of the matchup data, such as on plan position indicator (PPI) image displays (e.g., Fig. 4).

One set of output matchup variables is concerned with the reflectivity and rain-rate characteristics of the geometrically coincident, full-resolution PR and GR radar range gates included in their respective volume averages. These ''expected–rejected'' variables provide a metric that can be used to assess the ''goodness'' of the matchup between the radars. For a given PR ray and GR sweep,

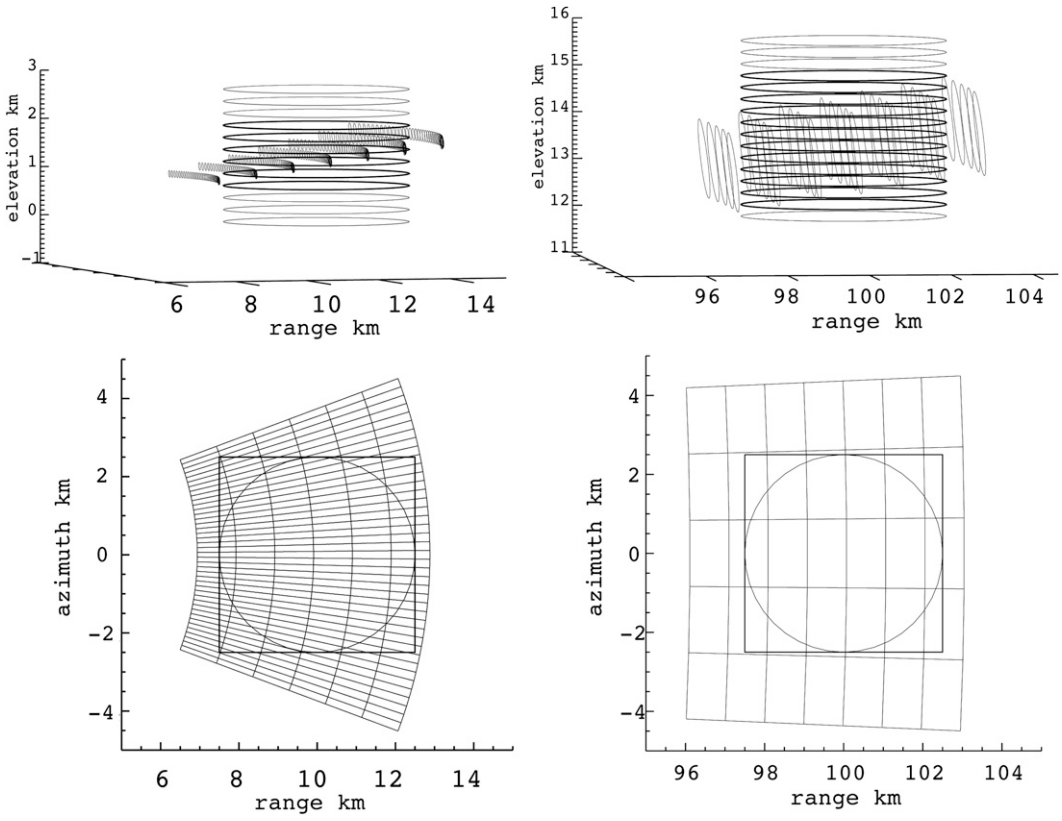

FIG. 3. (top) Illustration of the intersection of TRMM PR and WSR-88D GR sample volumes in the (left) near and (right) far range. (bottom) The projection of these intersections along a PR ray.

several GR range gates and rays will typically intersect several PR range gates, as illustrated in the vertical cross section in Fig. 3. The geometry-matching algorithm computes separate PR and GR volume-averaged values for all such intersecting PR and GR range gates, with the limitation that only those gates at or above specified reflectivity or rain-rate thresholds are included in the PR and GR gate averages. This reflectivity threshold, while selectable, is typically set at 18 dBZ for PR (the minimum sensitivity level of the TRMM PR) and 15 dBZ for ground radars. Individual PR or GR samples falling below this threshold are ''rejected,'' that is, they are not included in the matchup volume averages. When generating volume average reflectivity and rain-rate values for each matchup volume, the VN algorithm calculates (i) the number of PR and GR gates *expected* to be included in the averages from a strictly geometric standpoint, and (ii) the number of these PR and GR gates falling below the applicable measurement threshold and *rejected* from inclusion in the averages. These metrics are stored in variables in the matchup netCDF file. In statistical analyses of the data, effects of nonuniform beam filling and biases related to the detection threshold of the PR may be minimized by limiting the data points to those where the number of rejected gates is zero for both the GR and PR volume averages. See Fig. 4 for an example of the effect of limiting the matchup data based on the percent of rejected points in the sample averages.

The GPM validation network data product user's guide (NASA 2009) provides detailed descriptions of the VN netCDF matchup data file format and content, including a more detailed description of the gates expected–rejected variables. Copies of the user's guide are available online from the GPM ground validation web site (online at http://gpm.gsfc.nasa.gov/groundvalidation.html).

5. VN software and operations requirements

The VN software system exists as a set of Linux shell scripts, PostgreSQL database utilities, SQL commands, and a body of code written in Interactive Data Language (IDL; online at http://www.ittvis.com). The PR subset product and coincidence table data acquisition from the PPS, and cataloging, preprocessing, metadata extraction, and storage for these products are automated within the VN software. GR data receipt and cataloging are

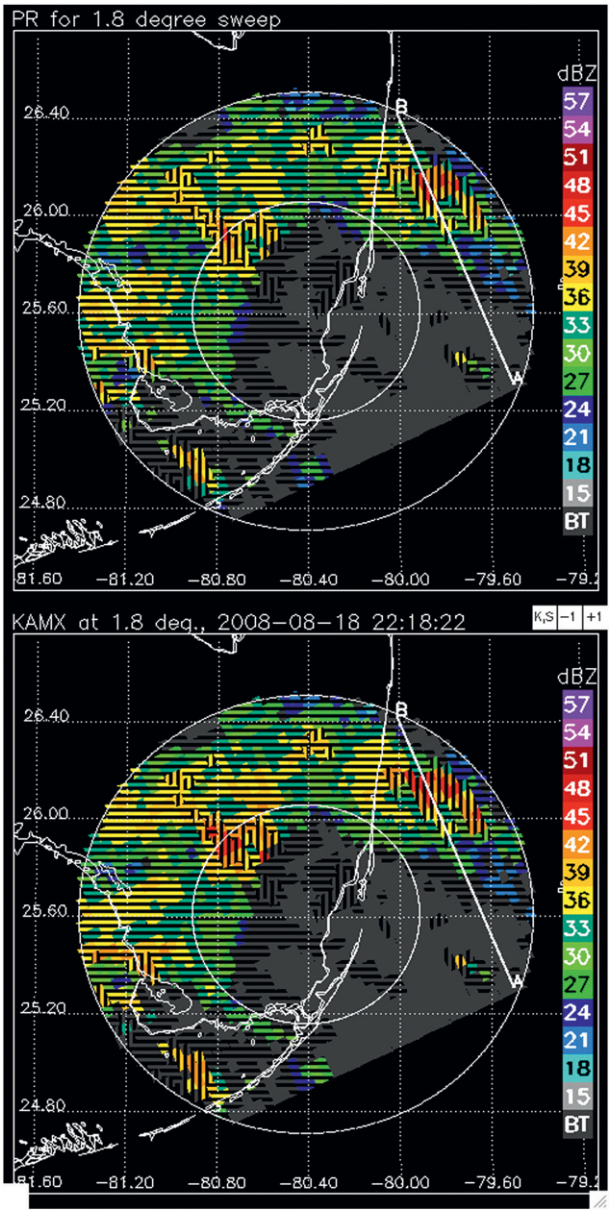

FIG. 4. (top) Geometrically matched PR and (bottom) KAMX WSR-88D data for the 1.8° elevation sweep of KAMX radar at 2218 UTC 18 Aug 2008, rendered as PPIs. Data samples shown are restricted to those points in common where at least 95% of the gates making up the sample averages were above fixed thresholds of 18 dBZ for PR and 15 dBZ for GR. Hatching shows PR-indicated rain type: vertical for convective, horizontal for stratiform. Rejected data points are shown (hatched pattern with dark gray color). Range rings are at 50 and 100 km. Edge of PR data swath is seen as the blank area to the south-southeast and inside 100 km. Line labeled A–B indicates the location of the vertical cross sections shown in Fig. 7.

automated for the WSR-88D sites, internal to the VN system, while WSR-88D data acquisition, quality control, and transmission to the VN system is a mix of automated and manual procedures, and is externally handled for the VN by the TRMM Ground Validation Office at NASA Goddard Space Flight Center (GSFC). Primarily because of security constraints, GR data acquisition and processing for other GR sites are currently performed manually on an ad hoc basis as data are made available by the provider, and use supporting scripts written for this purpose. Generation of the VN PR–GR matchup products is also performed on an ad hoc basis, though it may be readily automated to meet timeliness requirements for the data in the GPM era.

The driving system requirements for the ability to run the VN software are IDL running under Linux, UNIX, or Mac OS X. The PostgreSQL relational database management system (RDBMS) is required only for the operational data ingest, cataloging, and preprocessing component of the VN software suite, and is optional for the matchup product generation and statistical analysis and graphical display components. A different RDBMS could be substituted for PostgreSQL with minor software modifications. The Windows operating system is not supported by the baseline VN software. All VN processing and visualization software are designated "open source," and are available from the NASA GSFC Innovative Partnerships Program Office Web site (online at http://opensource.gsfc.nasa.gov).

The VN data processing system and database are designed with the flexibility to add additional data products, ground radar sites, and metadata parameters. Any ground radar sites within the TRMM PR area of coverage may be supported within the current system as long as the reflectivity data are available in a format compatible with the TRMM Radar Software Library in IDL (online at http://trmm-fc.gsfc.nasa.gov/index.html).

6. Visualization tools for case studies

A suite of visualization tools was developed for viewing and analyzing the VN geometry matchup datasets for individual site-overpass events. The two primary tools are the statistical analysis tool and the vertical cross-sectional tool. Noting that the matchup data are organized in the vertical by the elevation sweeps of the ground radar, with the horizontal sampling defined by the (ray and scan) coordinates of the TRMM PR, the data lend themselves to rendering as traditional PPI images. As with traditional PPI images from a scanning ground radar, the height above ground and the vertical depth of the matchup samples plotted in the PPI display increase with distance from the ground radar.

An example of the PPIs of PR and GR reflectivity rendered from the geometry match data for a rainy TRMM PR overpass event at KAMX (Miami, Florida, WSR-88D) for TRMM orbit 61300 around 2218 UTC 18 August 2007 is shown in Fig. 4. The figure shows PR and GR PPIs corresponding to the 1.8° elevation sweep of the ground radar, where the plotted matchup samples have been restricted to those where, for both the PR and GR, fewer than 5% of the gates averaged to produce the sample were rejected as being below fixed thresholds (18 dBZ for PR and 15 dBZ for GR) defined in the matchup algorithm. In this case of widespread, predominantly stratiform precipitation the effect of the threshold restriction is minimal. Figure 4 is an example of the interactive PPI image display as output by the vertical cross-sectional tool. All example displays and statistics below are based on attenuation-corrected PR data from the TRMM 2A-25 product.

The statistical analysis tool also displays user-selected PPIs as shown in Fig. 4, in the form of an animation loop progressing from low- to high-elevation sweeps. The statistical analysis tool stratifies the event data into vertical layers in the following two manners: 1) by height above the surface, in 1.5-km-deep layers, for 13 levels centered from 1.5 to 19.5 km; and 2) into three layers defined by proximity to the bright band (freezing level): above, within, and below the bright band. For purposes of the latter, a mean brightband height is computed from the brightband analysis in the TRMM PR 2A-25 product. A simple average of the 2A-25 brightband height as used in this analysis occasionally overestimates the observed brightband height in the PR reflectivity when the fraction of the area with a well-defined bright band is small, and errors in computed GR beam heights may occur in cases of nonstandard refractivity. Thus, for purposes of the statistical analysis of the matchup data, the brightband area of influence is extended to twice the upper range (~750 m) of observed brightband thickness (Fabry and Zawadzki 1995) to reduce the possibility of including brightband-affected data samples in the above- or below-brightband category. Matchup samples are categorized as above (below) the bright band if their base (top) is 750 m or more above (below) the mean brightband height. The remaining points are assigned as within the bright band.

The statistical analysis tool uses the vertically stratified data to produce a number of tabular and graphical displays. The upper left panel in Fig. 5 shows vertical profiles of PR (thick lines) and GR (narrow lines) reflectivity from matchup data averaged over the constant height levels. The remaining three panels in Fig. 5 display histograms of PR and GR reflectivity accumulated in 2-dBZ bins for matchup data stratified by proximity to the bright band: below (upper-right panel), within (lower left), and above (lower right). Table 2 presents PR–GR mean difference statistics output by the statistical analysis tool for data at the constant height levels broken out by rain type. The tool produces the same statistics broken out by proximity to the bright band (BB). Separate profile and histogram plots are produced for sample points identified as stratiform (solid lines) and convective (dotted lines) rain type, as well as for all points without regard to rain type (optional; not shown). Figure 6 shows the scatterplots of PR and GR reflectivity produced by the statistical analysis tool. Again the data are stratified by rain type and proximity to the bright band. The data samples included in Figs. 5 and 6 are limited to where at least 95% of the gates averaged to produce the matchup samples are above fixed reflectivity thresholds for both the PR and GR sample.

Both the vertical profile and histograms show good agreement between the PR and GR reflectivities for stratiform rain samples above and below the bright band in the mean. PR–GR reflectivity bias, computed as the mean difference for matching points, was −0.85 dBZ for the stratiform points below the bright band, and −0.43 dBZ for the stratiform points above the bright band, with near-identical reflectivity distributions. The vertical profiles for this stratiform subset of samples exhibits a characteristic frequently seen in the case of a well-formed bright band, in that the S-band GR profile is more affected by the presence of the bright band than the Ku-band PR profile. Note that the jump in GR reflectivity near the brightband level in the stratiform profile in Fig. 5 is much more pronounced than that for the PR. The mean PR–GR reflectivity difference for stratiform rain increases to −1.76 dBZ for points within the bright band.

The scatter diagrams in Fig. 6 show that there can be significant differences between the PR and GR matchup samples on a point-by-point basis, though the data heavily cluster along the 1:1 line. These differences are due to a combination of factors, including differences in viewing geometry, radar frequencies, and observation times; errors in vertical (for GR) and horizontal (for PR) geolocation of the data; and errors in the PR attenuation correction. The tools allow the S- to Ku-band frequency adjustment of Liao and Meneghini (2009) to be applied to the GR reflectivity data for points above (snow correction) and below (rain correction) the bright band. If these corrections are applied (not shown), the PR–GR reflectivity bias degrades to −2.02 dBZ for the stratiform points below brightband case, but improves to −0.08 dBZ for the stratiform points above the bright band, indicating that the attenuation correction for the PR is undercorrecting relative to the ground radar measurement for this case.

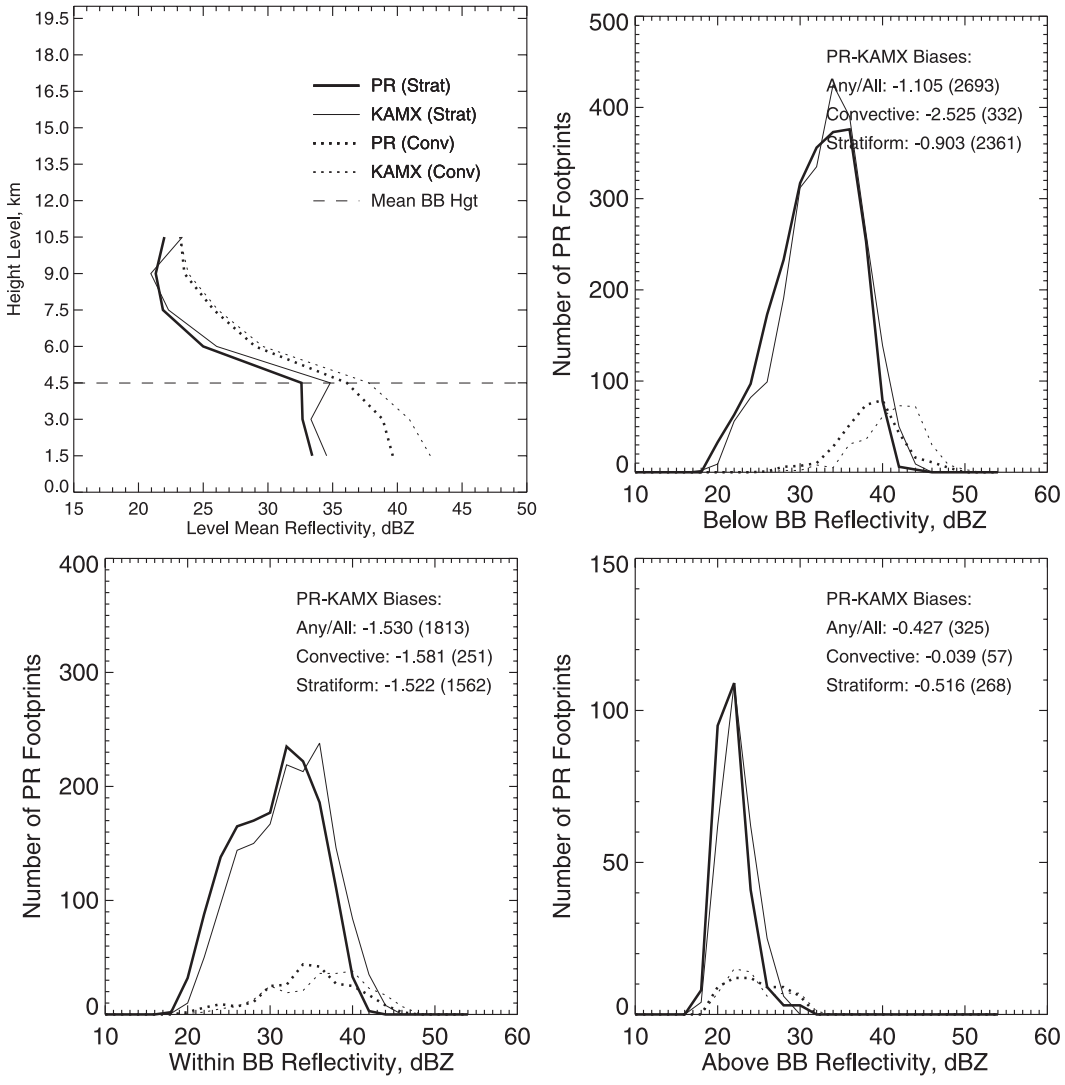

FIG. 5. (top left) Vertical profile and histograms of geometrically matched PR (heavy lines) and GR (narrow lines) reflectivity samples for the case shown in Fig. 4. Stratiform (solid) [convective (dotted)] rain type is plotted. Separate histograms are plotted for sample points (top right) below, (bottom left) within, and (bottom right) above the BB. Vertical scale varies in the histograms. PR–GR mean differences [bias (dBZ)] and sample sizes, by rain type, are indicated for the data in each histogram. Histogram bin width for accumulations is 2 dBZ. Points are limited to where at least 95% of the gates averaged to produce the PR and GR matchup samples are above fixed thresholds (see Fig. 4 and text). Dashed horizontal line in the vertical profile indicates the mean brightband height as analyzed in the TRMM PR 2A-25 product.

The vertical cross-sectional tool generates cross sections of the PR and GR reflectivity matchup data and PR–GR reflectivity difference along a selected PR scan line (perpendicular to the TRMM orbit track). Figure 7 shows vertical cross sections of PR reflectivity and PR–GR reflectivity difference for matchup data taken along the PR scan line indicated by the A–B line shown in Fig. 4, under the same data constraints as those in Figs. 4–6, but with the S- to Ku-band frequency adjustment applied to the GR reflectivity. The cross section passes through a convective core with matchup sample reflectivities up to 49 dBZ for the PR and 54 dBZ for the GR. The difference cross section shows that the per-sample PR reflectivity is generally within 1–2 dBZ of the GR above the brightband level, with the GR reflectivity exceeding the PR within and below the bright band, especially within the convective core.

The vertical cross-sectional tool in IDL is interactive, and its primary user interface is the PR–GR PPI image pair display, as shown in Fig. 4. Clicking the mouse on

TABLE 2. Vertical profile of PR–GR mean reflectivity difference (bias) and maximum PR and GR sample reflectivity for the case shown in Figs. 4 and 5. The asterisk at 4.5 km indicates the level under the influence of the bright band.

	Any type		Stratiform		Convective		PR max	GR max
Height (km)	PR bias	Total	PR bias	Total	PR bias	Total	reflectivity (dBZ)	reflectivity (dBZ)
1.5	−1.341	1251	−1.110	1096	−2.902	155	48.949	50.952
3.0	−0.828	1502	−0.650	1313	−2.053	189	46.439	50.640
4.5*	−2.162	990	−2.229	868	−1.695	122	45.684	46.522
6.0	−0.963	497	−1.041	415	−0.584	82	41.137	42.111
7.5	−0.400	81	−0.428	63	−0.313	18	30.208	32.672
9.0	0.037	12	0.384	6	−0.304	6	25.007	28.599
10.5	−0.654	2	−1.394	1	0.072	1	23.253	23.392

a point within the PPI image launches a new set of PR, GR, and PR–GR reflectivity cross sections along the PR scan line through the selected point. If the original 2A-25 TRMM PR product files are available, cross sections of full vertical resolution (250 m) PR data can also be displayed for comparison to the vertically averaged PR matchup data. Clicking on the labeled white boxes in the upper-right corner of the GR PPI allows the user to toggle the S- to Ku-band adjustment on and off, and increment and decrement the GR reflectivity in 1-dBZ steps to eliminate a known GR calibration offset from the cross-sectional displays. To investigate the quality of the PR and GR geometric alignment, the user can also click in the lower-left white box to launch a PPI animation sequence of PR and GR matchup data, and, if the data files are available, the full-resolution GR PPIs created from the original GR data volume.

7. Grouped analysis of VN data

The previous section described the VN tools that are available for analyzing individual rain events. This section examines collections of events to compute the bias between the TRMM PR and the NOAA WSR-88D Ground Radars on a station-by-station basis, and on the VN dataset as a whole.

a. Ground radar calibration comparisons

One potentially useful application of the VN data is to track the absolute calibration of ground radars over time. Table 3 presents the PR–GR bias (mean difference) for individual ground radars, for both the frequency-corrected GR reflectivity and the original S-band GR reflectivity. This dataset contains all of the samples categorized as stratiform rain type, with bottoms 750 m or more above the bright band, where the percentage of PR and GR range gates rejected as ''below threshold'' in the sample averages is below 5%. Events where fewer than five points meet the criteria were excluded from the analysis.

The frequency-corrected biases for most radar sites in Table 3 are less than 1 dBZ, with a few notable exceptions. KGRK (Fort Hood, Texas) shows a positive PR–GR bias over the full dataset, indicating a negative calibration offset in the KGRK radar relative to other WSR-88D sites. Several adjacent WSR-88D sites near or along the Gulf Coast between Louisiana and Florida (KLCH, KLIX, KSHV, KTBW, and KTLH) exhibit a PR–GR bias of −1 dBZ or lower, indicating a positive calibration offset of the WSR-88D radar. This set of Gulf Coast radars, KEVX and KMOB excepted, seem to be well calibrated to one another, but run ''hot'' compared to the other WSR-88D sites in the VN subset.

Figure 8 shows a time series of mean PR–GR reflectivity differences for each WSR-88D site in the VN, and for the University of Alabama, Huntsville, ARMOR dual-polarimetric C-band radar (labeled RMOR) from July 2006 through March 2009. Figure 8 uses the same criteria as in Table 3 (stratiform rain, above bright band, having 5% or fewer range gates below threshold in sample averages), with the additional constraint that, to reduce noise, at least 25 sample points must meet the criteria for the event to be included in the plot. A simple average of the event-by-event biases plotted in Fig. 8 cannot be directly compared to the accumulated mean biases in Table 3, because Table 3 takes the number of samples in each event into account in the mean difference computations, and the number of qualifying samples per event can vary by over an order of magnitude.

While KGRK shows a negative GR bias with respect to the PR over the full dataset as seen in Table 3, Fig. 8 shows that the events with the consistently negative biases occur prior to mid-2007, but KGRK improved to near-0 mean bias after mid-2007. KGRK and RMOR are the only sites that show a clear trend in the GR calibration. It is known that the calibration of the ARMOR data provided to the VN was improved between the early events and the later dates (W. Petersen 2008, personal communication). Several sites (KAMX, KBYX, KCRP, and KMLB) show consistent, small biases with

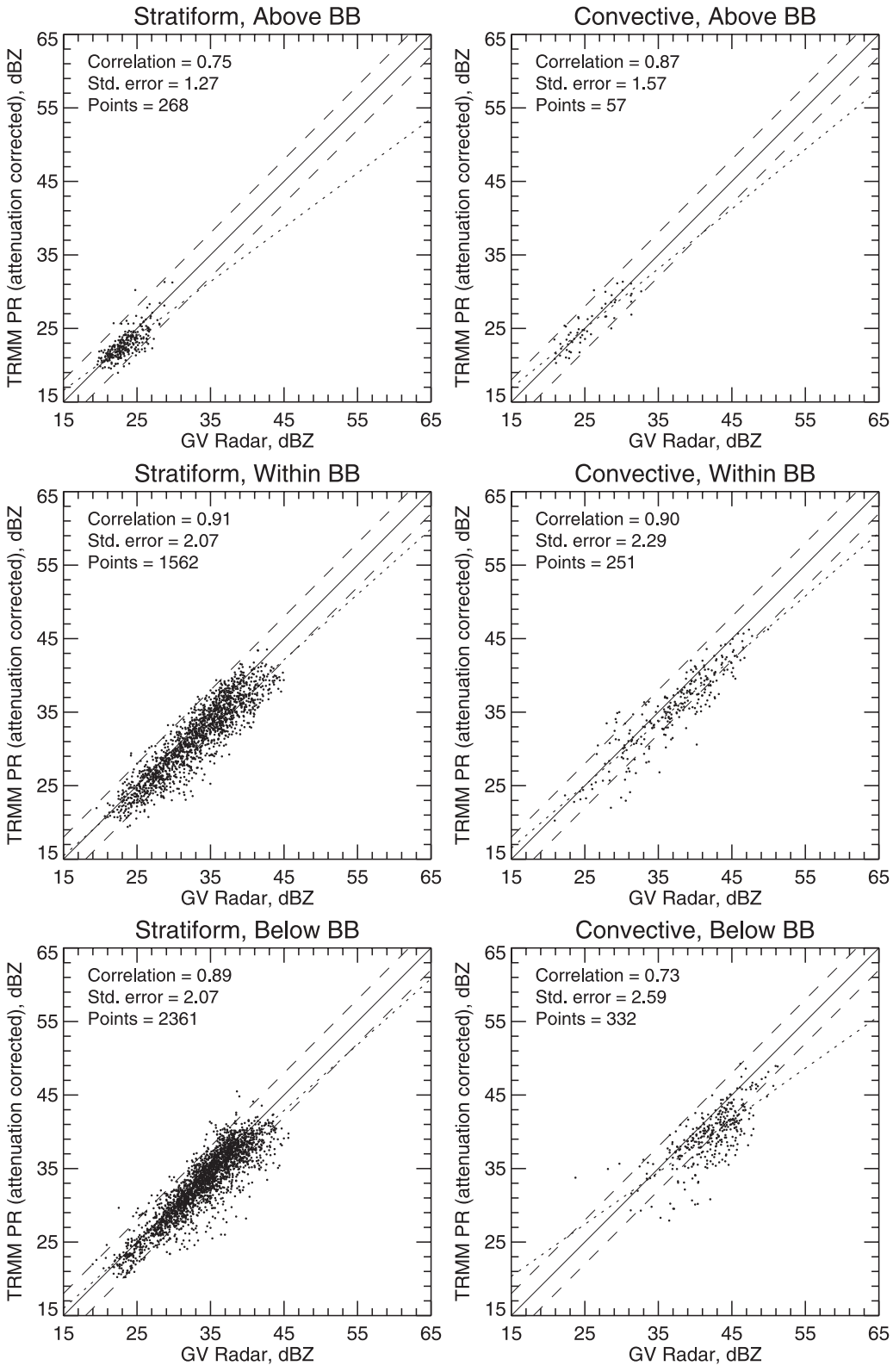

FIG. 6. Scatterplots of PR vs GR reflectivity for the case and data constraints shown in Figs. 4 and 5. The 1:1 match (solid lines), ±3-dBZ bounds (dashed lines), and the linear fit to the data (dotted lines): (top) above and (bottom) within BB; (left) stratiform and (right) convective.

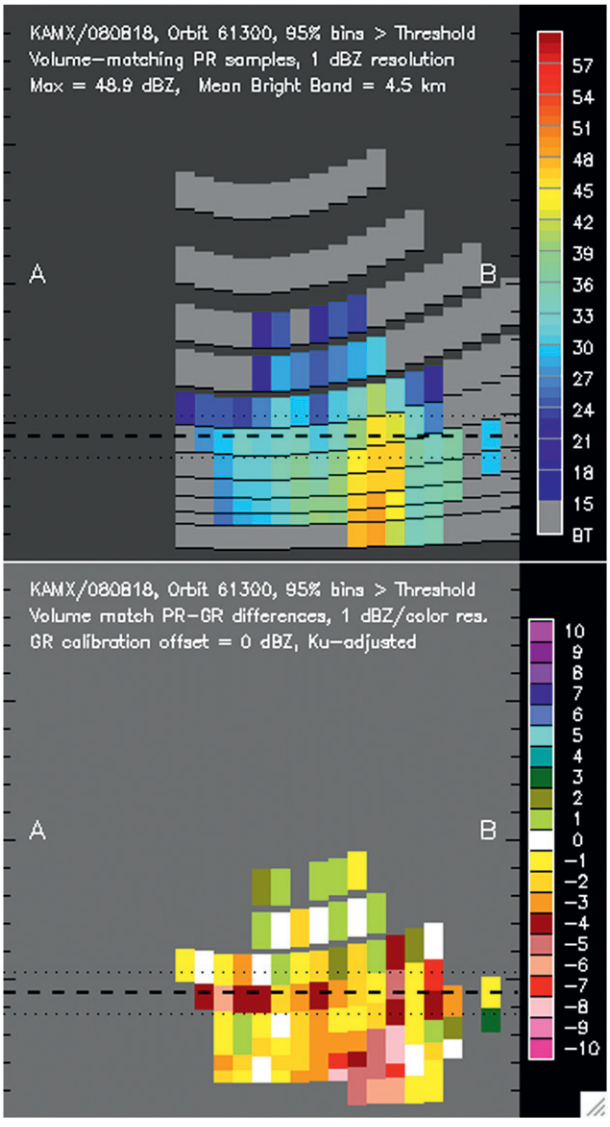

FIG. 7. Vertical cross section, from 0–20-km height, of (top) PR reflectivity and (bottom) PR–GR reflectivity difference from geometrically matched PR and GR data along the PR scan line labeled A–B in Fig. 4. GR data have had S- to Ku-band adjustments applied. PR data (gray) show sample points rejected based on the threshold criteria of Fig. 4. Vertical extent of samples in the lower elevation sweeps has been adjusted to eliminate overlaps in the plots. The mean brightband height (heavy dashed line); plotted 750 m above and below this height is the area of influence of the bright band (dotted lines; see text).

respect to the PR, indicating a stable calibration of those WSR-88D systems. These sites also generally have fewer rainy events meeting the criteria for inclusion, which may help reduce the variability.

b. Analysis of PR bias

The analysis described here evaluates PR bias compared to the VN WSR-88D ground radars (Table 1) in terms of reflectivity factor and rain rate for PR version 6 data collected during the period from 8 August 2006 through 25 March 2009. This period of record starts at the beginning of VN operations and ends prior to the date of the PR instrument anomaly that occurred on 29 May 2009. This anomaly caused a cessation of instrument operations until 17 July 2009, and data collected after this date were subject to a change in calibration when the instrument was reactivated. The dataset for this analysis was further restricted by the following:

- the inclusion of only significant rain events (as defined in section 3) over the U.S.WSR-88D ground radars;
- the omission of KGRK data because, as described above, it appears that the calibration of the station changed considerably over the period of record of the dataset;
- the inclusion of the PR sample volumes only where reflectivity factor exceeded 18 dBZ for all of the range gates included in the average, and where 18 dBZ is the instrument's minimum usable sensitivity;
- the inclusion of the GR sample volumes only where reflectivity factor exceeded 15 dBZ for all of the range gates included in the average (to match the PR's sensitivity, allowing for up to −3-dBZ calibration offset of the GR); and
- the use of data only from the period prior to 26 March 2009, excluding data acquired just prior to and following the PR instrument anomaly that occurred on 29 May 2009.

The radar frequency corrections defined by Liao and Meneghini (2009) were applied to the GR data to account for the differences in reflectivity factor that occur when the same rain or snow targets are observed by S- and Ku-band radars. The snow correction was applied to data above the bright band, and the rain correction was applied to the data samples below the bright band.

Figure 9 illustrates the distribution of the PR–GR bias as a function of the attenuation correction applied to the PR data. The applied attenuation correction was calculated as the average of the corrected PR reflectivity factor in a matchup data volume minus the average of the raw PR reflectivity factor in the same volume. Negative values for the amount of attenuation correction applied are most likely due to cases where the PR algorithm's surface reference technique is applied to light rain events, and the algorithm calculates a negative path-integrated attenuation (J. Kwiatkowski 2010, personal communication). The corrected and raw values were obtained from the TRMM 2A-25 and the 1C-21 data products, respectively. In the figure, data are divided into convective and stratiform cases from high in the atmosphere (>5.75 km above ground level) and low in the

TABLE 3. Mean PR instrument bias compared to WSR-88D GR measurements for stratiform rain samples from above the melting layer, by GR site. The bias was calculated as the mean difference (PR–GR) of reflectivity factor for matchup samples. Bias estimates are shown for both frequency-corrected GR data (GR_{Ku}) and uncorrected GR data. The sample size is identified for each site.

Radar ID	PR–GR_{Ku} mean difference (dBZ)	PR–GR mean difference (dBZ)	PR mean reflectivity (dBZ)	Ku-adjusted GR mean reflectivity (GR_{Ku}) (dBZ)	GR mean reflectivity (dBZ)	Total samples
KAMX	0.03	−0.49	22.65	22.63	23.14	2304
KBMX	−0.77	−1.47	23.9	24.67	25.37	12 194
KBRO	−0.51	−1.12	23.15	23.66	24.27	2009
KBYX	0.04	−0.49	22.77	22.74	23.26	1042
KCLX	−0.76	−1.42	23.54	24.3	24.96	9071
KCRP	0.51	−0.03	23.37	22.86	23.39	2808
KDGX	0.07	−0.53	23.65	23.58	24.18	7266
KEVX	−0.07	−0.68	23.61	23.68	24.29	6488
KFWS	0.97	0.43	23.78	22.81	23.35	11 910
KGRK	2.63	2.19	24.19	21.55	21.99	6871
KHGX	−0.09	−0.68	23.46	23.54	24.14	3332
KHTX	0.44	−0.16	23.96	23.52	24.12	12 141
KJAX	−0.72	−1.33	22.95	23.68	24.29	4509
KJGX	0.73	0.17	23.81	23.09	23.65	6569
KLCH	−1.34	−2.06	23.54	24.89	25.6	4071
KLIX	−1.46	−2.15	23.18	24.64	25.33	7955
KMLB	0.71	0.26	22.52	21.81	22.27	2787
KMOB	1.00	0.50	23.37	22.37	22.87	4772
KSHV	−1.04	−1.71	23.35	24.39	25.06	8000
KTBW	−0.98	−1.62	22.99	23.97	24.61	3309
KTLH	−1.62	−2.34	23.37	24.99	25.71	3280

atmosphere (from the lowest valid matchup volume up to 1.75 km above ground level).

As illustrated in the figure, the average PR–GR reflectivity factor bias is relatively low for the data collected high in atmosphere in the both the stratiform and convective cases: −0.68 and +0.03 dBZ, respectively. The PR–GR bias is relatively greater in the samples drawn from the lower part of the atmosphere. In the stratiform case, the average PR–GR reflectivity factor bias for the lower-atmosphere samples is −1.46 dBZ. In the convective case, the average bias is −1.88 dBZ for samples taken from the lower atmosphere. As observed in Fig. 9, the range of attenuation correction applied to the PR data by the 2A-25 algorithm is greatest for the case of convective samples taken from the lower part of the atmosphere. In this case, the path-integrated attenuation of the PR Ku-band signal is expected to be greater than in the other cases examined here, primarily due to the higher concentrations of cloud water, rain, and partially melted hydrometeors (Liao and Meneghini 2009). When the attenuation of the Ku-band signal is significant, the corrections applied by the TRMM PR algorithm can change the raw radar reflectivity factor by a factor of 10 or more compared to the corrected value (Iguchi et al. 2000). Again, using GR data corrected by the Liao and Meneghini (2009) method, and in the case of convective data sampled from lower in the atmosphere, PR–GR bias increases as the amount of attenuation applied to the PR data increases (Fig. 9, lower right panel). The bias starts at an average of −1.65 dBZ when the attenuation correction applied is between 0 and 2 dBZ, and the PR–GR bias steadily increases to −3.07 dBZ for cases where the attenuation correction applied is >6 dBZ (Fig. 9, lower right panel).

An evaluation was performed using the same dataset as described above to assess the bias of the PR rain rate compared to the rain rate estimated from WSR-88D ground radars. In this study, the bias was expressed as the ratio of the PR/GR rain rates. PR and GR reflectivity was converted to rain rate using the Z–R relationship, where $Z = 372R^{1.54}$ (Kozu et al. 2001). It is acknowledged that the choice of this Z–R relationship is somewhat arbitrary, but it is used here to illustrate how the bias observed in the PR radar reflectivity factor applies to rain rate.

Figure 10 illustrates the PR–GR rain-rate bias (as true bias) expressed as a series of atmospheric profiles. The average PR–GR bias is plotted at the height levels indicated in the figure. The thick lines (PRcor) are rain-rate bias calculated using 2A-25 attenuation-corrected PR reflectivity, and the thin lines (PRraw) represent the use of 1C-21 raw PR reflectivity. The solid lines (GR) represent the bias results calculated using the original GR values converted to rain rate. The dashed lines (GRadj) are the bias results obtained when the Liao and Meneghini (2009) frequency corrections were applied to the GR reflectivity before converting to rain rate. Data

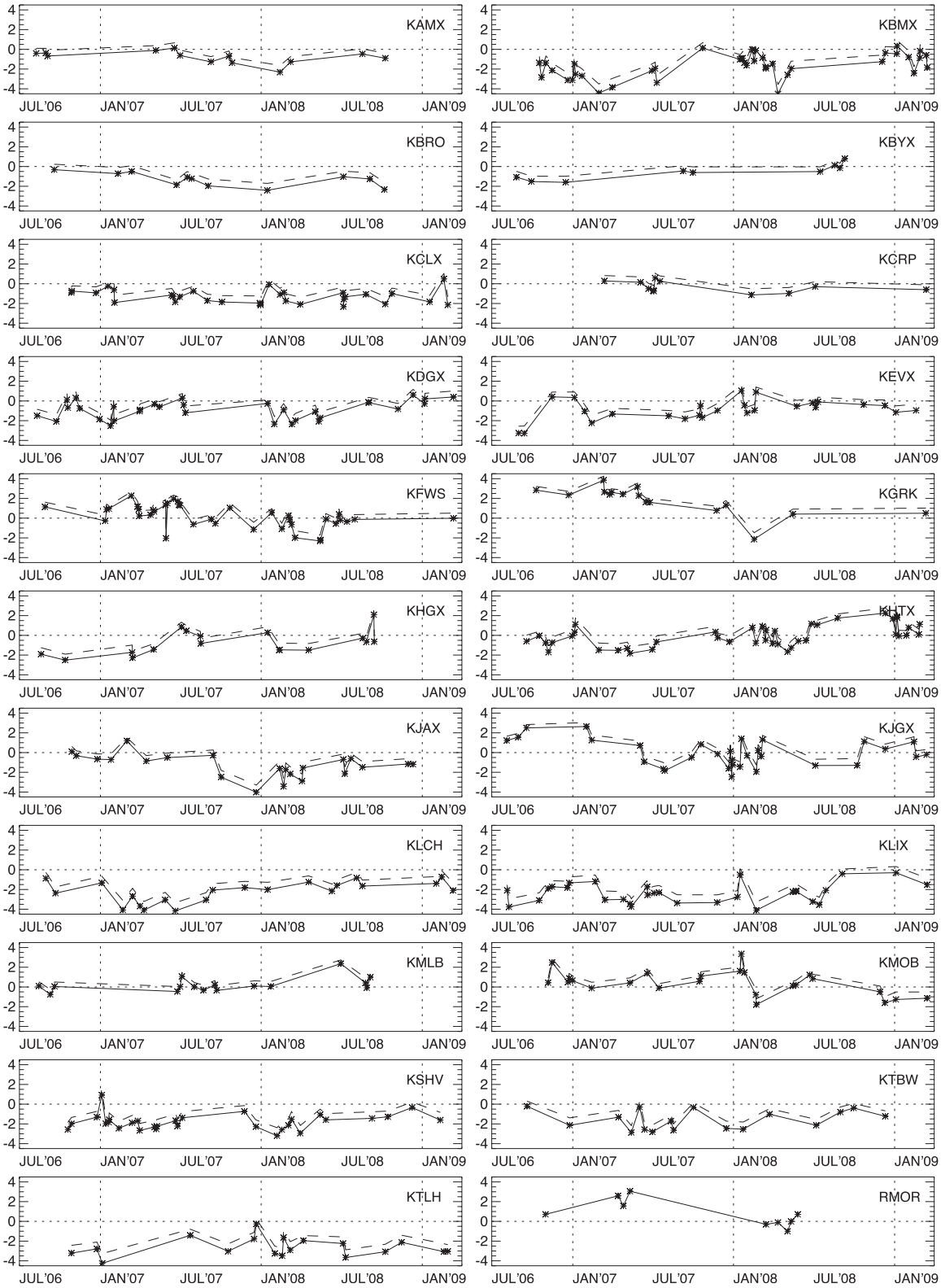

FIG. 8. Time series of PR–GR mean reflectivity differences for stratiform rain above the bright band. Individual rain event dates are shown by the asterisks. Differences based on unadjusted (solid line) and S- to Ku-band frequency adjusted (dashed line) GR. Only GR-unadjusted difference values are plotted for RMOR, a C-band radar.

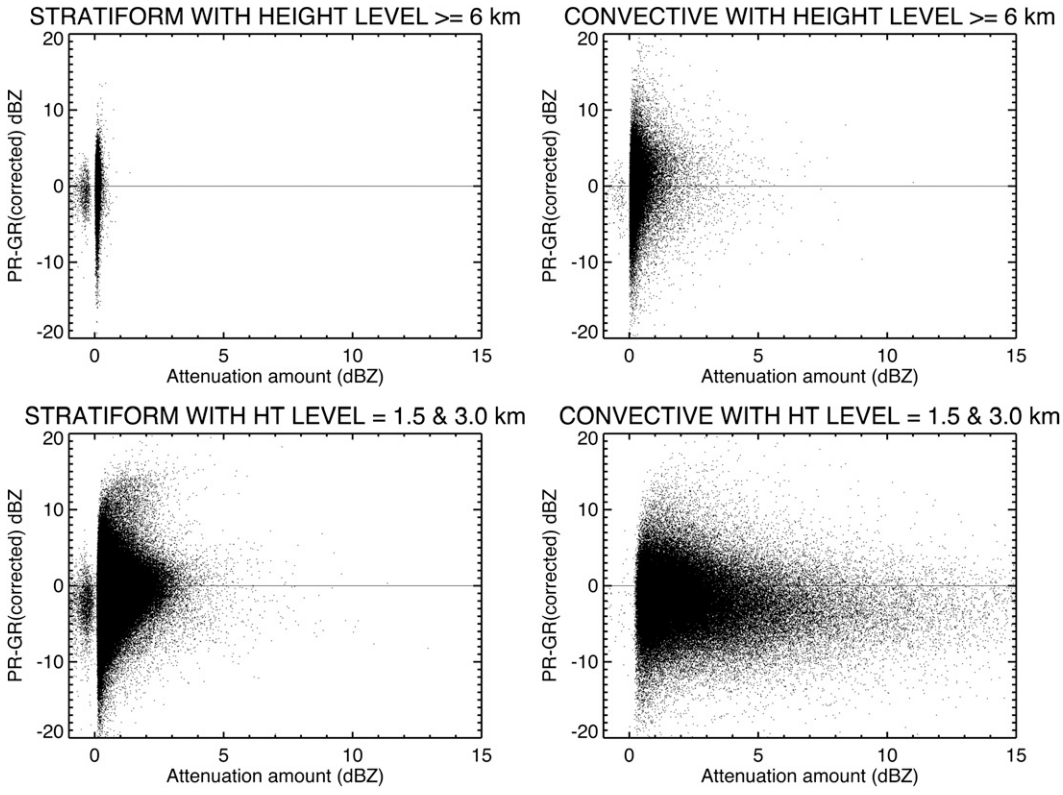

FIG. 9. Scatterplot of PR minus GR radar reflectivity factor compared to the amount of attenuation correction applied to the PR data for VN matchup samples measured over the WSR-88D radars identified in Fig. 1 (excluding KGRK, see text), over the VN period of record until 25 Mar 2009. Samples from (right) convective and (left) stratiform cases taken from the (top) upper and (bottom) lower parts of the atmosphere. The 0-bias line is plotted. Frequency corrections were applied to the GR data (Liao and Meneghini 2009).

samples affected by the bright band are excluded from the profiles. In all cases, the PR–GR rain-rate bias improves in the snow–ice regions at upper levels with the application of the frequency corrections to the GR reflectivity, averaging slightly greater (less) than unity for convective (stratiform) rain. In the rain–liquid regions at lower levels, both the convective and stratiform PR–GR rain-rate biases are below unity, increasingly so after application of the frequency corrections to the GR reflectivity. As illustrated in Fig. 10, the PR underestimates rain rate by 30%–40% compared to frequency-corrected GR samples taken from the lower part of the atmosphere. These results indicate an undercorrection of attenuation for the PR reflectivity in the mean for PR version 6, particularly in convective situations, as also seen by Liao and Meneghini (2009) in comparing the PR to the Melbourne, Florida, WSR-88D.

8. Summary and conclusions

As described above, the Validation Network is an integral part of the Ground Validation System for NASA's Global Precipitation Mission (GPM). In the GPM prelaunch era, the VN supports precipitation retrieval algorithm development. Postlaunch, the VN will be used to validate GPM spacecraft instrument measurements and retrieved precipitation data products.

Several examples are provided above that demonstrate how the VN dataset can be used to compare ground- to space-based radar reflectivity for validation purposes. Examples include comparisons in individual storms, in a time series of storms over individual ground radars, and in a multiyear aggregate of storms over the entire southeast United States.

Analysis of individual storms illustrates several of the key features of the VN. Chief among these is the ''matchup'' method that permits direct comparison of volume-averaged ground- and space-based radar data. The VN algorithm averages the minimum number of full-resolution space and ground radar bins needed to produce spatially coincident sample volumes. Space-based radar data are averaged only along each vertical ray, between the top and bottom height of each ground radar elevation sweep that it intersects (Fig. 2). Ground radar

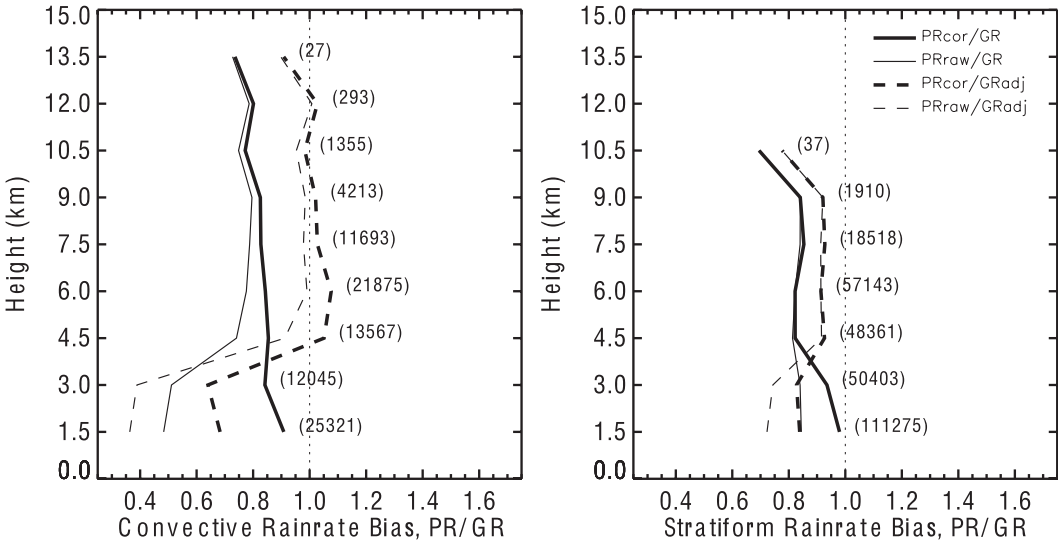

FIG. 10. Vertical profiles of (left) convective and (right) stratiform mean rain-rate bias (PR–GR) from volume-matched reflectivity data grouped by height, using $Z = 372R^{1.52}$, and excluding samples affected by bright band. Heavy (narrow) lines use attenuation-corrected 2A-25 (raw 1C-21) PR reflectivity. Original (solid lines) [frequency adjusted (dashed lines)] GR reflectivity is used. Number of samples in each height layer is shown next to the profiles. No-bias (=1.0) line is shown (light dotted line). Data for VN matchup samples measured over the WSR-88D radars identified in Fig. 1 (excluding KGRK, see text), over the VN period of record until 25 Mar 2009.

data are averaged only in the horizontal within the individual elevation sweeps that intersect the space radar rays' parallax-adjusted profiles (Fig. 3). The result of this technique is a set of vertical profiles for a given rainfall event, at the PR horizontal resolution and location and the GR vertical resolution and location, with coincident space and ground radar samples located at essentially random heights along each individual profile (Fig. 7). There is no data interpolation, extrapolation, or resampling to a regular grid.

The analysis of individual storms also illustrates the standard VN products generated for each rain event. These include PPI images, vertical profiles, histograms, scatter diagrams, and mean difference statistics for PR and GR reflectivity, as shown in Figs. 4–6 and Table 2. It should be noted that data points included in the standard matchup that generated these figures (and the other analysis described here) are limited to those that fall within a 100-km radius centered on the ground radar. By 115 km, radar systems with a 1° beamwidth (such as WSR-88D) will have a vertical resolution >2 km, which is considered too coarse for meaningful comparisons with the space-based radar data, such as those available from TRMM and GPM.

Examples provided above also illustrate the utility of the VN dataset as a means for assessing the long-term calibration of ground radars. The period of record for the VN prototype begins on 8 August 2006 and runs to the present for the 21 ground radar sites located in the southeast United States (Fig. 1). Table 3 and Fig. 8 show that for this period of record the frequency-corrected bias between the TRMM PR and WSR-88D GR is less than 1 dBZ in most cases, with several notable exceptions. For example, it was found that several adjacent WSR-88D sites near or along the Gulf Coast between Louisiana and Florida exhibit a PR minus GR reflectivity factor bias of −1 dBZ or lower, indicating a high calibration offset for these WSR-88D ground radars. This set of Gulf coast radars (KEVX and KMOB excepted) appears to be well calibrated to one another, but run "hot" compared to the other WSR-88D sites in the VN subset. Further investigation is required to determine whether these results represent actual calibration offsets, or to what degree the Gulf Coast meteorological regime contributes to the observed offsets.

An assessment was also made of the PR-to-GR bias measured over a period of record of 960 days for 20 of the 21 WSR-88D radars illustrated in Fig. 1. The analysis found a remarkably small difference between PR and GR radar reflectivity factor averaged over this period of record in stratiform and convective rain cases when samples were taken from high in the atmosphere. A significant difference in PR and GR reflectivity was found in convective cases, particularly in convective samples from the lower part of the atmosphere. In this case, the mean difference between PR and corrected GR reflectivity was −1.88 dBZ. The PR–GR bias was found to increase with the amount of PR attenuation correction

applied, with the PR–GR bias reaching −3.07 dBZ in cases where the attenuation correction applied is >6 dBZ (Fig. 9, lower-right panel). Additional analysis indicated that the version 6 TRMM PR retrieval algorithm underestimates rainfall in case of convective rain in the lower part of the atmosphere by 30%–40% (Fig. 10).

Several steps have been taken to make the VN dataset as accessible as possible for GPM algorithm development and for data product validation. Summary data products are available for each precipitation event. Ground radar data in several common formats can be ingested into the VN, including Universal Format (UF) and the WSR-88D level II archive data format. The volume-matched VN data are output in netCDF, a portable, self-describing data format that is commonly used in the atmospheric sciences. A data user's guide is available, which details the VN netCDF data file-naming conventions, format, and contents. Space- and ground-radar matchup data are available for each significant rain event, and all original PR and WSR-88D GR data products are available for these and all other overpass events. VN data and documentation are available via NASA's GPM ground validation Web site (online at http://gpm.gsfc.nasa.gov/ground_direct.html). VN data visualization tools are available that render the matchup data in vertical ''plan position indicator'' slices through the data or as vertical cross sections, and provide reflectivity difference statistics and additional graphical renderings. The VN volume matching code and visualization tools, written in Interactive Data Language (IDL), are available as open source software from the NASA GSFC Innovative Partnerships Program Office Web site (online at http://opensource.gsfc.nasa.gov).

Additional data will certainly be added to the VN as the period of record expands. Enhancements to the VN are also planned, with the possibility of expanding the period of record to dates earlier than 8 August 2006, and with the possibility of adding additional data types, including space-based microwave radiometer data, as well as additional data derived from various precipitation retrieval methods. Community contributions that improve and enhance the open source VN software are welcome, as are contributions of ground radar data from additional sites. Updates to the VN will be documented on the GPM ground validation Web site (http://gpm.gsfc.nasa.gov/groundvalidation.html). This site provides a portal to VN contacts, data, software, and documentation, as well as to other ground validation datasets, both within and beyond GPM.

Acknowledgments. The Validation Network is supported as part of NASA's Global Precipitation Measuring Mission. The authors wish to acknowledge the contributions of Jason Pippitt from the TRMM Ground Validation office, who performs quality control of the ground radar data used in the VN. We also gratefully acknowledge the ground radar data provided by Jun Park and Mi-Lim Ou of the Korean Meteorological Administration (Gosan radar), Walter Petersen of NASA's Marshall Space Flight Center (ARMOR radar), Elizabeth Ebert from the Australian Bureau of Meteorology (Darwin radar), and David Wolff of NASA's Goddard Space Flight Center (Kwajalein radar).

REFERENCES

Anagnostou, E. N., C. A. Morales, and T. Dinku, 2001: The use of TRMM Precipitation Radar observations in determining ground radar calibration biases. *J. Atmos. Oceanic Technol.,* **18,** 616–628.

Barnes, S. L., 1980: Report on a meeting to establish a common Doppler radar data exchange format. *Bull. Amer. Meteor. Soc.,* **61,** 1401–1404.

Bolen, S. M., and V. Chandrasekar, 2000: Quantitative cross validation of space-based and ground-based radar observations. *J. Appl. Meteor.,* **39,** 2071–2079.

——, and ——, 2003: Methodology for aligning and comparing spaceborne radar and ground-based radar observations. *J. Atmos. Oceanic Technol.,* **20,** 647–659.

Fabry, F., and I. Zawadzki, 1995: Long-term radar observations of the melting layer of precipitation and their interpretation. *J. Atmos. Sci.,* **52,** 838–851.

GCOS, 2006: Systematic observation requirements for satellite-based products for climate: Supplemental details to the satellite-based component of the ''Implementation Plan for the Global Observing System for Climate in Support of the UNFCCC.'' GCOS Rep. GCOS-107 and WMO/TD 1338, 103 pp. [Available online at http://www.wmo.int/pages/prog/gcos/Publications/gcos-107.pdf.]

Hou, A. Y., G. Skofronick-Jackson, C. D. Kummerow, and J. M. Shepherd, 2008: Global precipitation measurement. *Precipitation: Advances in Measurement, Estimation and Prediction,* S. C. Michaelides, Ed., Springer-Verlag, 131–170.

Iguchi, T., T. Kozu, R. Meneghini, J. Awaka, and K. Okamoto, 2000: Rain-profiling algorithm for the TRMM Precipitation Radar. *J. Appl. Meteor.,* **39,** 2038–2052.

Keenan, T., K. Glasson, F. Cummings, T. S. Bird, J. Keeler, and J. Lutz, 1998: The BMRC/NCAR C-band polarimetric (C-POL) radar system. *J. Atmos. Oceanic Technol.,* **15,** 871–886.

Kozu, T., and Coauthors, 2001: Development of precipitation radar onboard the Tropical Rainfall Measuring Mission (TRMM) satellite. *IEEE Trans. Geosci. Remote Sens.,* **39,** 102–116.

Kummerow, C., and Coauthors, 2000: The status of the Tropical Rainfall Measuring Mission (TRMM) after two years in orbit. *J. Appl. Meteor.,* **39,** 1965–1982.

Liao, L., and R. Meneghini, 2009: Changes in the TRMM version-5 and version-6 precipitation radar products due to orbit boost. *J. Meteor. Soc. Japan,* **87A,** 93–107.

——, ——, and T. Iguichi, 2001: Comparisons of rain rate and reflectivity factor derived from the TRMM Precipitation Radar and the WSR-88D over the Melbourne, Florida, site. *J. Atmos. Oceanic Technol.,* **18,** 1959–1974.

NAS, 2007: *Earth Science and Applications from Space: National Imperatives for the Next Decade and Beyond*. National Academy Press, 456 pp.

NASA, 2009: Validation network data user's handbook, 28 pp. [Available online at http://gpm.gsfc.nasa.gov/ground_library.html.]

Neeck, S. P., and R. Oki, 2007: CEOS precipitation constellation. *Proc. SPIE,* **6744,** 674428, doi:10.1117/12.746142.

NOAA/OFCM, 2006: Doppler radar meteorological observations: Part C WSR-88D products and algorithms. Federal Meteorological Handbook No. 11 (FCM-H11C-2006), Office of the Federal Coordinator for Meteorological Services and Supporting Research, National Oceanic and Atmospheric Administration, 390 pp. [Available online at http://www.ofcm.gov/fmh11/fmh11partc/pdf/FMH-11-PartC-April2006.pdf.]

Park, S.-G., and D.-K. Lee, 2007: Doppler weather radar network over the Korean peninsula. Preprints, *33rd Conf. on Radar Meteorology,* Cairns, QLD, Australia, Amer. Meteor. Soc., P11A.5. [Available online at http://ams.confex.com/ams/pdfpapers/123031.pdf.]

Petersen, W. A., K. R. Knupp, D. J. Cecil, and J. R. Mecikalski, 2007: The University of Alabama Huntsville THOR Center instrumentation: Research and operational collaboration. Preprints, *33rd Int. Conf. on Radar Meteorology,* Cairns, QLD, Australia, Amer. Meteor. Soc., 5.1. [Available online at http://ams.confex.com/ams/pdfpapers/123410.pdf.]

Rosenfeld, D., E. Amatai, and D. B. Wolff, 1995: Classification of rain regimes by the three-dimensional properties of reflectivity fields. *J. Appl. Meteor.,* **34,** 198–211.

Schumacher, C., and R. A. Houze Jr., 2000: Comparison of radar data from TRMM satellite and Kwajalein oceanic validation site. *J. Appl. Meteor.,* **39,** 2151–2164.

Simpson, J., C. Kummerow, W.-K. Tao, and R. F. Adler, 1996: On the Tropical Rainfall Measuring Mission (TRMM). *Meteor. Atmos. Phys.,* **60,** 19–36.

Wolff, D. B., D. A. Marks, E. Amitai, D. S. Silberstein, B. L. Fisher, A. Tokay, J. Wang, and J. L. Pippitt, 2005: Ground validation for the Tropical Rainfall Measuring Mission (TRMM). *J. Atmos. Oceanic Technol.,* **22,** 365–380.